Journal of Organometallic Chemistry, 280 (1985) 407–418
Elsevier Sequoia S.A., Lausanne – Printed in The Netherlands

GENERAL THEORETICAL ANALYSIS OF THREE-CONNECTED POLYHEDRAL MOLECULES AND THEIR CAPPED DERIVATIVES

ROY L. JOHNSTON and D. MICHAEL P. MINGOS*

Inorganic Chemistry Laboratory, University of Oxford, South Parks Road, Oxford OX1 3QR (Great Britain)

(Received August 14th, 1984)

Summary

Stone's Tensor Surface Harmonic Theory has been successfully applied to three-connected polyhedral molecules of the Main Group and transition elements. The skeletal molecular orbitals consist of four (S^σ and P^σ) radial bonding molecular orbitals, $(n-4)/2$ bonding $L^\pi(L>1)$ surface molecular orbitals and $(n-2)L^\pi$ and $\overline{L}^\pi$ matching non-bonding molecular orbitals. These molecules have $3n/2$ skeletal molecular orbitals and are characterised by a total of $5n$ valence electrons. The corresponding transition metal polyhedral molecules are characterised by $15n$ electrons.

The development of the cluster chemistries of the Main Group and transition metals has been assisted by the formulation of simple electron counting rules described collectively as the Polyhedral Skeletal Electron Pair Approach [1–3]. These rules are summarized in Table 1. The theoretical basis of the rules has been examined using a range of theoretical techniques. Generally these have been based on specific MO calculations or graph theoretical approaches [4,5].

Stone [6–9] has developed an elegant methodology based on spherical harmonics with scalar, vector and tensor properties (Tensor Surface Harmonic Theory) which has neatly accounted for the bonding characteristics of deltahedral molecules. In the Tensor Surface Harmonic analysis clusters are treated as sets of atoms distributed over the surface of a sphere. The position of each atom (i) is defined by the angular coordinates (θ_i, φ_i). The frontier orbitals of E–H (E = B or C), or *isolobal* fragments [10], comprise one inward pointing (radial) hybrid and two tangential p (or dp hybrid) orbitals which may lie along the line of increasing θ (p^θ) or φ (p^φ).

Values of the scalar harmonics [6] $Y_{lm}(\theta_i,\varphi_i)$ at each atom i are used as the coefficients in an LCAO expansion (with the basis set being the radial atomic hybrid orbitals σ_i) generating a set of n cluster MOs (where n is the number of atoms in the cluster).

$$\Psi^\sigma_{lm} = \sum_{i=1}^{n} Y_{lm}(\theta_i,\varphi_i)\sigma_i$$

0022-328X/85/$03.30

TABLE 1

SUMMARY OF POLYHEDRAL SKELETAL ELECTRON PAIR APPROACH[a] POLYHEDRAL ELECTRON COUNT (p.e.c.)

Polyhedral type	Main Group	Example	Transition metal	Example[b]
Deltahedra (*closo-*)	$4n+2$	$B_nH_n^{2-}$	$14n+2$	$Os_5(CO)_{16}$
nido-	$4n+4$	B_nH_{n+4}	$14n+4$	$Ru_5C(CO)_{15}$
arachno-	$4n+6$	B_nH_{n+6}	$14n+6$	$[Os_4H_3I(CO)_{12}]$
Three-connected polyhedra	$5n$	C_nH_n	$15n$	$Ir_4(CO)_{12}$
Ring compounds	$6n$	C_nH_{2n}	$16n$	$Os_3(CO)_{12}$
Condensed polyhedra derived from A (p.e.c. a) and B (p.e.c. b)[c]				
Vertex shared	$a+b-18$			
Edge shared	$a+b-34$			
Δ-face shared	$a+b-48$			

[a] D.G. Evans and D.M.P. Mingos, Organometallics, 2 (1983) 435. [b] B.F.G. Johnson and J. Lewis, Phil. Trans. R. Soc. Lond., A308, (1982) 5. [c] D.M.P. Mingos, J. Chem. Soc., Chem. Commun., (1983) 706.

The quantum numbers l and m are analogous to those obtained in the solution of the Schrödinger equation for the hydrogen atom. The skeletal MOs are designated L_m^{σ}, where L represents one of the symbols S, P, D... according to $l = 0,1,2....$

L_m^{π} and $\bar{L}_m^{\pi}$ cluster MOs are obtained by taking the vector surface harmonics V_{lm}^{θ} and V_{lm}^{φ} as LCAO expansion coefficients, where the basis set is now the set of p^{θ} and p^{φ} orbitals. $2n$ p^{θ}/p^{φ} orbitals give rise to nL^{π} and $n\bar{L}^{\pi}$ surface MOs. These orbitals have the opposite symmetry under inversion and are related by an operation

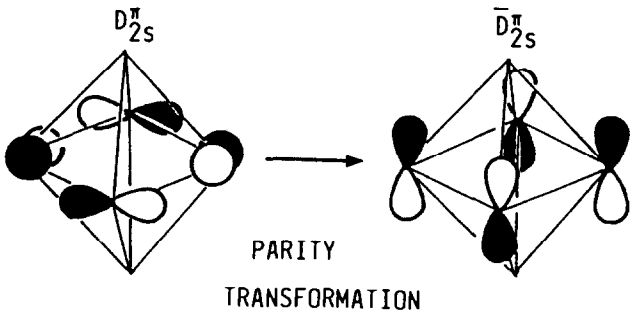

(1)

described as a *parity transformation*. This involves the rotation, in the same sense, of each atomic p orbital in an L_m^{π} MO by 90° about a radial axis passing through the atom. The corresponding $\bar{L}_m^{\pi}$ MO is generated by this operation as shown in **1**.

Stone's approach accounts in a very general manner for the $4n+2$ electron rule for Main Group deltahedral clusters [7] ($14n+2$ for the corresponding transition metal compounds). Deltahedral geometries are preferred for "electron deficient" Main Group clusters because they maximize the number of nearest neighbour bonding interactions. The $n+1$ skeletal bonding MOs associated with these mole-

cules arise from four strongly bonding radial ($S^\sigma + 3P^\sigma$) MOs (though the P^σ orbitals have a significant amount of P^π character mixed into them) [11] and $n - 3L^\pi$ ($L > 1$) surface MOs.

Not all spherical polyhedral molecules have $4n + 2$ electrons, however. The three-connected molecules illustrated in Fig. 1 represent an important general class and are characterized by $5n$ electrons [12] ($15n$ for transition metal clusters). These electron counts correspond to a total of $3n/2$ occupied skeletal MOs.

Although the bonding in such compounds has been described in localized terms [13] it is instructive to contrast the general bonding features of deltahedral and three-connected polyhedra within the same molecular orbital framework.

An inspection of ab initio and semi-empirical molecular orbital calculations on the molecules C_nH_n [14] has shown that three-connected spherical polyhedra have four strongly bonding ($S^\sigma + 3P_\sigma$) radial MOs, and in addition have $(n/2) - 2$ bonding L^π and $(n - 2)L^\pi$ and $\bar{L}^\pi$ non-bonding surface MOs making a total of $3n/2$ skeletal MOs. (Details of these calculations are given in Appendix I). The different molecular orbital patterns for deltahedral and three-connected polyhedra are summarized in Fig. 2. Clearly the deltahedral provide the minimum number of skeletal MOs and the three-connected polyhedra the maximum number consistent with an approximately, spherical distribution of bonded skeletal atoms.

The deltahedra thereby maximize the degree of delocalization and the three-connected polyhedra maximize the degree of localization of skeletal electron pairs. Indeed the latter exhibit a 1 : 1 mapping of skeletal MOs and polyhedral edges, which leads to their alternative description as "electron precise" polyhedra [2].

Clearly the major difference between the two classes of clusters arises from differences in the bonding properties of the L^π and $\bar{L}^\pi$ surface MOs in the two cases.

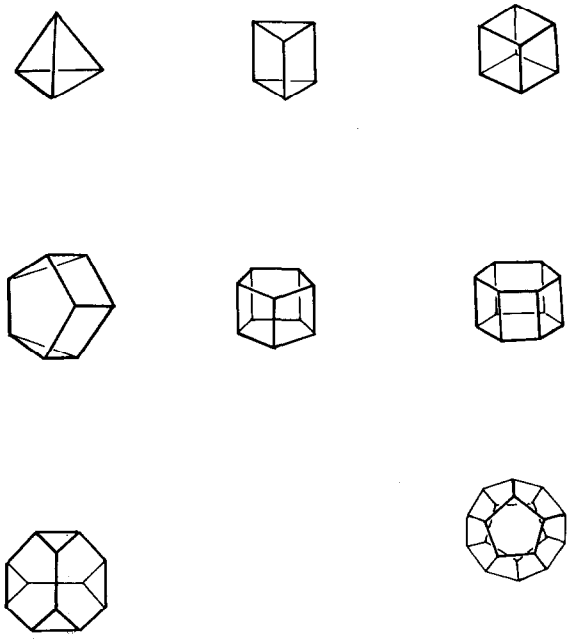

Fig. 1. Some examples of three-connected polyhedra.

For illustrative purposes the bonding D^{π} MOs (of t_{2g} symmetry) of an octahedron and their antibonding $\overline{D}^{\pi}(t_{2u})$ counterparts are depicted in Fig. 3(a), along with the $D^{\pi}(a_1' + e'')$ and $\overline{D}^{\pi}(a_1'' + e')$ MOs of a trigonal prism. In this specific example rotation of the bottom triangle, so as to eclipse the top triangle of atoms, results in the stabilization of the two e' components of $\overline{D}^{\pi}(1s,1c)$ and the destabilization of two e'' components of $D^{\pi}(1s,1c)$ resulting in a set of 4 $(n-2)$ non-bonding MOs, see Fig. 3(b). The formation of matching pairs of non-bonding L^{π} and $\overline{L}^{\pi}$ MOs is a direct consequence of their relationship through the *parity transformation*, which reverses the bonding characteristics of an MO (see **1**). Strongly bonding L_m^{π} MOs have matching strongly antibonding $\overline{L}_m^{\pi}$ MOs and weakly bonding L_m^{π} MOs weakly antibonding $\overline{L}_m^{\pi}$ MOs. In the case of the tetrahedron the D^{π} and $\overline{D}^{\pi}$ orbitals are exactly non-bonding and therefore form a degenerate pair of e MOs. For higher nuclearity polyhedra the $(n-2)L^{\pi}$ and $\overline{L}^{\pi}$ orbitals are only approximately non-bonding.

The geometric feature which most clearly and generally distinguishes deltahedra and three-connected polyhedra is the relative disposition of atoms in successive layers. The former have staggered and the latter eclipsed arrangements of atoms.

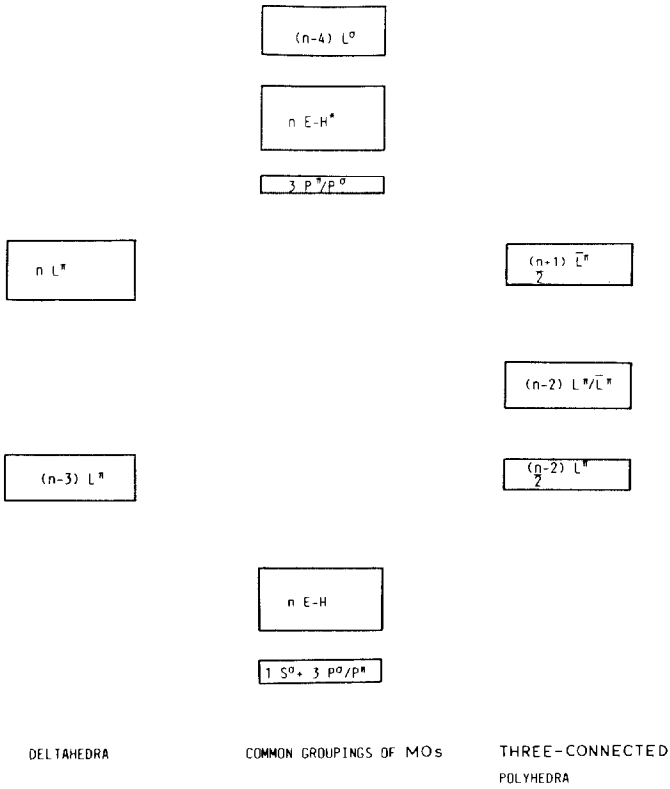

Fig. 2. A schematic representation of the molecular orbitals for deltahedral and three-connected polyhedral E_nH_n molecules (E = a Main Group atom). Molecular orbitals common to both classes of molecule are illustrated in the centre. The differences in skeletal MO bonding patterns arise primarily from the L^{π} and $\overline{L}^{\pi}$ $(L > 1)$ functions. The $(n-2)L^{\pi}/\overline{L}^{\pi}$ MOs of the three-connected polyhedral molecules are essentially non-bonding.

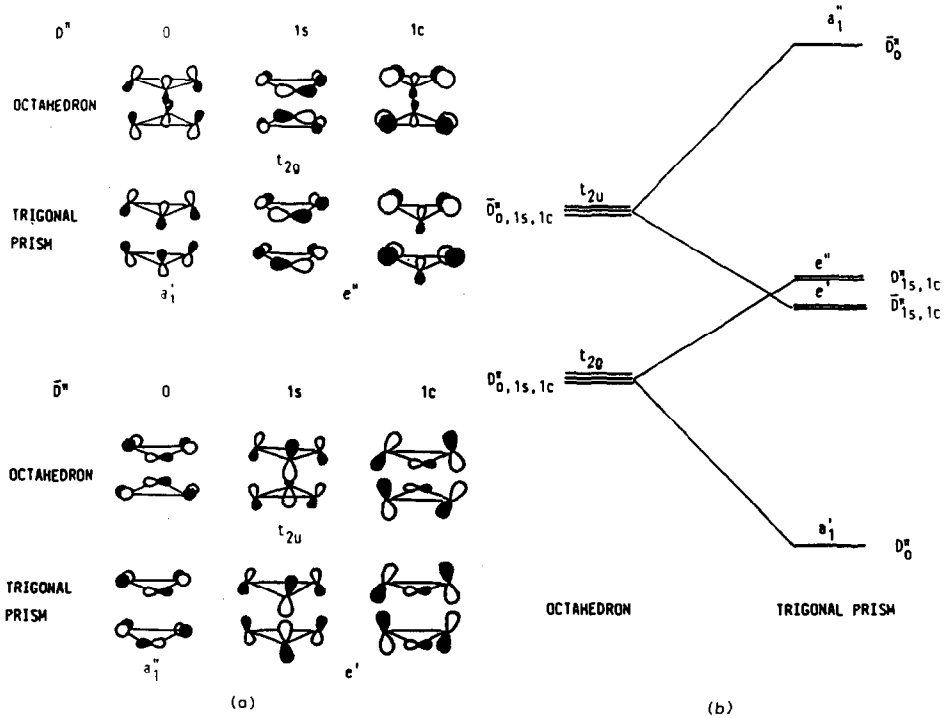

Fig. 3. The D^{π} and $\bar{D}^{\pi}$ MOs of a trigonal prism and an octahedron are contrasted in (a) and their relative energies represented in (b).

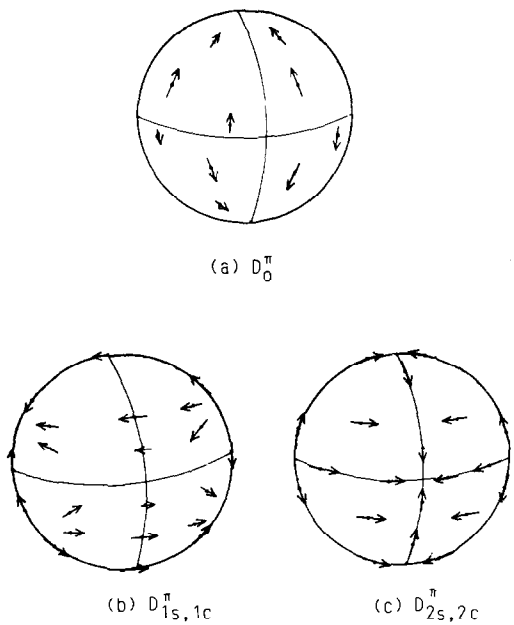

Fig. 4. Schematic representation of the D^{π} vector surface harmonics (a). The arrows in the Figures represent the relative phases and magnitudes of p orbitals functions of the vertex atoms. For $D^{\pi}_{1s,1c}$(b) only one component is illustrated, the second component is related to that shown by a 90° rotation about the polar axis. Similarly for $D^{\pi}_{2s,2c}$ (c) the two components are related by a 45° rotation about the polar axis.

Three-connected polyhedra therefore have horizontal mirror planes between layers of atoms, whereas deltahedra have no such mirror planes. Consequently the different bonding properties of L^{π} and $\bar{L}^{\pi}$ MOs, in the two structure types, must be related to differences in bonding character across the equator of the sphere on which the atoms lie. Figure 4 illustrates the D^{π} vector surface harmonics in a simplified and general fashion. The arrows in the Figure represent the relative phases and magnitudes of the atomic p orbital functions [6–9]. As indicated above it is sufficient merely to explain why certain of the D^{π} functions become non-bonding for three-connected polyhedra since the corresponding $\bar{D}^{\pi}$ functions must also be non-bonding because of the properties of the parity transformation.

From Fig. 4(a) it is apparent that the D_0^{π} function has p^{θ} orbitals pointing towards the poles of the sphere. The orbital interactions across the equator are bonding as the function posesses a horizontal mirror plane. Figure 5(a) illustrates the fact that the bonding interactions will be similar for the D_0^{π} MOs of clusters with staggered or eclipsed geometries and that in both cases the orbital will be bonding. The only case for which this is not true is the tetrahedron, which is simultaneously

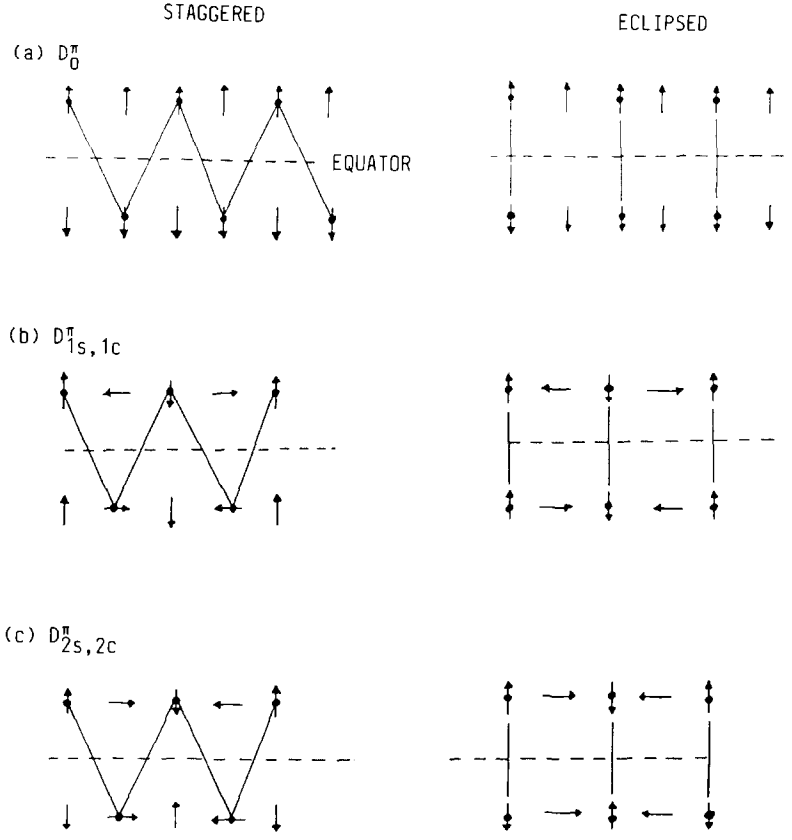

Fig. 5. Schematic illustration of the bonding characteristics across the equator of D^{π} functions for staggered and eclipsed arrangements of atoms. For D_0^{π} (a) both the staggered and eclipsed arrangements give bonding interactions. For $D^{\pi}_{1s,1c}$ (b) the interactions are bonding for staggered and anti-bonding for eclipsed. See text for discussion of $D^{\pi}_{2s,2c}$ (c). The sign inversions occur every 180° for D_1^{π} and every 90° for D_2^{π}.

three-connected and a deltahedron. The D_0^π orbital of the tetrahedron takes the form illustrated in **2a**. Because the top and bottom layers are staggered by 90° the cross-equator interaction is π-antibonding. The $\overline{D}_0^\pi$ orbital is also non-bonding and degenerate with it (**2b**). The function is overall non-bonding because the cross-equator interaction is bonding.

For $D_{1s,1c}^\pi$ functions there is no mirror plane through the equator, but instead the equator forms a nodal plane (Fig. 4(b)). Analysis of the bonding characteristics of these functions for staggered and eclipsed geometries (Fig. 5(b)) reveals that, whereas in the former case the cross-equator interactions are bonding, in the latter they are antibonding. It is these antibonding interactions which make the $D_{1s,1c}^\pi$ MOs non-bonding for all prisms. These orbitals are bonding within the planes above and below the equator and antibonding across the equator, thereby making them non-bonding in total. If, however, more layers are added to the structure then the $D_{1s,1c}^\pi$ orbitals become bonding because eclipsed atoms on the same side of the equator (Fig. 4(b)) have p orbitals interacting in-phase.

A trigonal prism has three D^π MOs–D_0^π bonding and $D_{1s,1c}^\pi$ non-bonding. The addition of two more atoms to form a cube leads to the formation of two additional MOs based on the D^π functions ($D_{2s,2c}^\pi$) shown in Fig. 4(c). These functions are related by a 45° rotation about the polar axis. The cube has atoms eclipsed in planes above and below the equator, disposed at 90° intervals around the sphere. The $D_{2s,2c}^\pi$ functions may be considered (Fig. 5(c)) as having a p^θ component with maximum in-plane antibonding character at 90° intervals (vertical arrows in Fig. 5(c)) and a p^φ component with maximum in-plane bonding character at 90° intervals (horizontal arrows). These two components are 45° apart and both are bonding across the equator. D_{2c}^π has p^θ components at $\theta = 0$, 90, 180, 270° whereas D_{2s}^π (rotated by 45° relative to D_{2c}^π) has p^φ components at these angles. Therefore it can be seen that D_{2c}^π is antibonding within the upper and lower layers but bonding across the equator; therefore it is overall non-bonding. In contrast the D_{2s}^π orbital is bonding within and between the layers and is overall bonding. The square-antiprisms has the upper and lower layers staggered by an angle of 45° so that (Fig. 5(c)) both the $2s$ and $2c$ functions have p^θ components only on one side of the equator and p^φ components on the other, making one layer bonding and the other anti-bonding. The cross-equator interactions are bonding. The result is to make the $D_{2s,2c}^\pi$ pair of orbitals degenerate and overall bonding for the antiprism. The non-bonding D_{2c}^π orbital in the prism becomes more bonding in the antiprism, while the originally strongly bonding D_{2s}^π orbital becomes less bonding.

For the three-connected polyhedral clusters with more than eight atoms both of the D_2^π orbitals are bonding. That this is so may readily be understood by considering the pentagonal and hexagonal prisms. There are now in each layer more than four atoms so that their φ angles differ by less than 90°. This means that for the D_{2c}^π function the atoms are not at the positions for maximum in-plane antibonding interaction. For the pentagonal prism the non-bonding L^π functions are $D_{1s,1c}^\pi$ and $F_{2s,2c}^\pi$. The $F_{2s,2c}^\pi$ functions are illustrated in **3**. Since they have a nodal plane passing through the equator, their similarity to $D_{1s,1c}^\pi$ can be readily appreciated. The hexagonal prism has an extra non-bonding F_{3c}^π orbital which is similar to D_{2c}^π in the case of the cube. The $F_{3s,3c}^\pi$ MOs of the hexagonal prism (Fig. 6) are both bonding across the equator (possess a horizontal mirror plane) but one is bonding within the upper face and the other is antibonding.

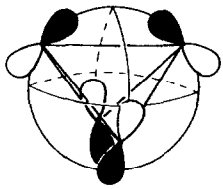

(2a) D_0^{π}

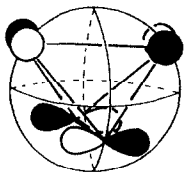

(2b) $\bar{D}_0^{\pi}$

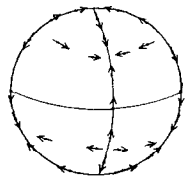

(3) F_{2s}^{π} (F_{2c}^{π} rotate by 45°)

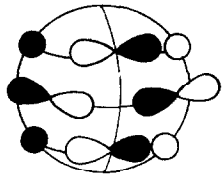

(4)

The analysis above has demonstrated the occurrence of the following L^{π} non-bonding orbitals: 1-tetrahedron, 2-trigonal prism, 3-cube, etc., i.e. $(\frac{n}{2}-1)L^{\pi}$. Since these must be matched by an equal number of $\bar{L}^{\pi}$ MOs, it follows that these polyhedra have $n-2$ non-bonding molecular orbitals associated with them. In addition they have $(n-4)/2$ bonding L^{π} MOs and four S^{o} and P^{o} MOs (See Appendix II for details). Therefore the total number of MOs for three-connected polyhedral molecules is:

$$(n-2)+(n-4)/2+4=3n/2$$

It follows that Main Group three-connected polyhedral molecules are characterized by $5n$ electrons and transition metal polyhedral molecules by $15n$ electrons. Table 2 gives specific examples of these types of polyhedral molecules.

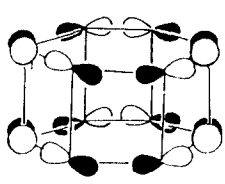

(a) F_{3s}^{π}

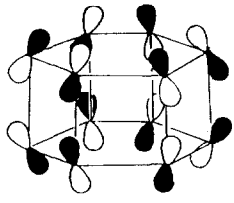

(b) F_{3c}^{π}

Fig. 6. The $F_{3s,3c}^{\pi}$ pair of molecular orbitals for a hexagonal prism.

TABLE 2

EXAMPLES OF THREE-CONNECTED POLYHEDRAL MOLECULES

No. of Vertex atoms n	Geometry	Example	Electron count
(a) Main Group examples (5n electrons)			
4	Tetrahedral	$C_4(^tBu)_4$ [12a] P_4, As_4 $Sn_2Bi_2^{2-}$	20
6	Trigonal prism	C_6H_6 [12b] (prismane)	30
8	Cube	C_8H_8 (cubane) [12c]	40
	Cuneane	C_8H_8 (cuneane)	
10	Pentagonal prism	$C_{10}H_{10}$ [12d] (pentaprismane)	50
20	Dodecahedron	$C_{20}H_{20}$ [12e] (dodecahedrane)	100
(b) Transition metal examples (15n electrons)			
4	Tetrahedral	$Ir_4(CO)_{12}$ [15a]	60
6	Trigonal prism	$[Rh_6C(CO)_{15}]^{2-}$ [15b]	90
8	Cube	$[Ni_8(PPh)_6(CO)_8]$ [15c]	120
8	Cuneane	$[Co_8S_2(N^tBu)_4(NO)_8]$ [15d]	120

Capped cluster molecules

The arguments developed above are particularly useful for analysing the bonding in capped three-connected polyhedral molecules. If, as is generally the case, the frontier orbitals of the capping atoms match the bonding and non-bonding skeletal MOs in symmetry then no new bonding or non-bonding skeletal MOs are introduced. This *capping principle* [16] leads to the following electron counts for Main Group and transition metal molecules: $5n + 2m$, and $15n + 12m$; where m is the number of capping atoms and n the number of atoms in the parent three-connected polyhedron.

When there are three or more capping atoms forming a ring their frontier orbitals generate a combination of the $\bar{P}_0^\pi$ type which is not matched by the occupied skeletal MOs (S^σ, P^σ, L^π, $\bar{L}^\pi$ ($L > 1$)) of the three-connected polyhedron. It can interact with an antibonding $\bar{P}_0^\pi$ skeletal MO, resulting in the presence of an additional weakly bonding $\bar{F}_0^\pi$ orbital. It generally has the symmetry a_2 for a C_{nV} point group and is schematically illustrated in **4**. Figure 7 shows part of the MO diagram for the specific example of a tricapped-trigonal prism. From the previous discussion it follows that a weakly bonding $\bar{F}_0^\pi$ orbital is parity-matched by a weakly antibonding F_0^π orbital. The $F_0^\pi(a_2'')$ MO results from overlap of the P_0^π function generated by the capping atoms with the P_0^π skeletal MO of the trigonal prism (see Fig. 7). Analysis of the bonding in the tetracapped cube (D_{4h} symmetry) has shown that this structure also has a frontier orbital pair consisting of a weakly bonding $\bar{F}_0^\pi$ MO and a weakly antibonding F_0^π MO.

In summary, capped three-connected-polyhedral clusters are characterized by electron counts of $5n + 2m$ ($15n + 12m$ for transition metals) unless the capping atoms form a ring, in which case the electron count can be either $5n + 2m + 2$ or $5n + 2m + 4$ (depending upon whether or not the weakly antibonding F_0^π orbital is occupied). For the tricapped trigonal prism this leads to electron counts of $4N + 2$ or

TABLE 3

EXAMPLES OF CAPPED THREE-CONNECTED POLYHEDRAL MOLECULES (m = no. of capping atoms)

n	m	Geometry	Example	Electron count
1. Based on tetrahedron (60 + 12m electrons)				
4	1	Trigonal bipyramid	$Os_5(CO)_{16}$ [17a]	72
4	2	Bicapped tetrahedron	$Os_6(CO)_{18}$ [17b]	84
4	3	Tricapped tetrahedron	$CoRu_3Au_3(PPh_3)_3(CO)_{12}$ [17c]	96
2. Based on trigonal prism (90 + 12m electrons)				
6	2	Bicapped trigonal prism	$Cu_2Rh_6C(CO)_{15}(NCMe)_2$ [17d]	114
3. Based on cube (120 + 12m electrons)				
8	5	Pentacapped cube	$[Rh_{14}(CO)_{25}]^{4-}$ [17e]	180

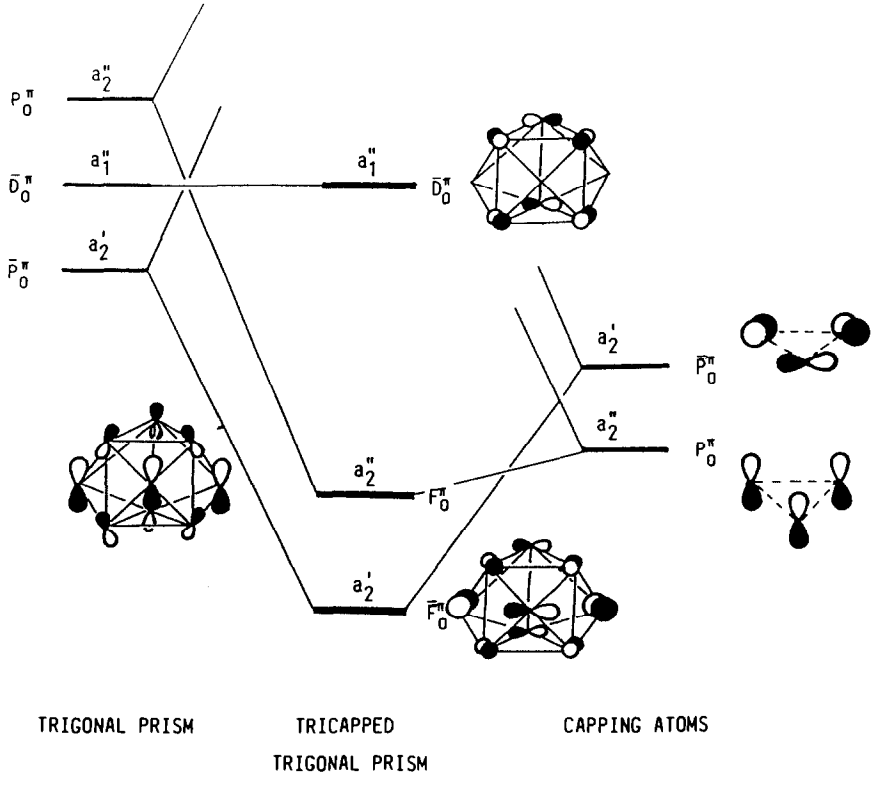

Fig. 7. Molecular orbital interaction diagram for a tricapped trigonal prism as which emphasises the role of the P_0^π and $\bar{P}_0^\pi$ functions on the capping atoms.

$4N + 4$ where $N = n + m$. Wade [18] and Corbett [19] have discussed the geometric consequences of these alternative electron counts for Main Group tricapped-trigonal prismatic molecules.

Examples of capped three-connected transition metal clusters are given in Table 3. The majority of these examples have $15n + 12m$ electrons because the capping atoms do not introduce any new symmetry types. The pentacapped centred cube has a ring of four capping atoms but retains an electron count of $15n + 12m$, i.e. 180. The calculations suggest the possibility of forming a more reduced species with either 181 or 182 electrons. This corresponds to filling of the F_0^π level. The tetracapped centred-pentagonal prism $[Rh_{15}C_2(CO)_{28}]^-$ [20], which has the four capping atoms forming a ring (three cap square faces and the other caps a pentagonal face), has an electron count of 200 ($15n + 12m + 2$). This is in agreement with the ideas developed above.

In summary the above analysis has demonstrated how the molecular orbitals of three-connected polyhedral molecules differ from those of deltahedra. The analysis has been based on the Stone Tensor Surface Harmonic Methodology. In a subsequent paper localised orbital schemes for three-connected polyhedra and deltahedra will be presented which also account for the differences in their electronic structures.

Acknowledgements

The S.E.R.C. is thanked for financial support.

Appendix I

Extended Hückel calculations were performed on the species C_4H_4 (T_d), C_6H_6 (D_{3h}) and C_8H_8 (O_h) and on the deltahedron C_6H_6 (O_h) and the *arachno*-(deltahedral fragment) C_8H_8 (D_{4d}). The bond lengths used were C–C 1.54 and C–H 1.09 Å.

PARAMETERS USED IN CALCULATIONS

Atom	Orbital	H_{ii} (eV)	ξ
C	2*s*	−21.4	1.625
	2*p*	−11.4	1.625
H	1*s*	−13.6	1.30

The Hückel constant k was taken as equal to 1.75. Ab initio and semi-empirical calculations quoted [14] were of the following types: STO-3G, 4-31G, SCF-Xα, MINDO/3 and INDO.

Appendix II

BONDING AND NON-BONDING SKELETAL MOs OF SOME THREE-CONNECTED POLYHEDRAL CLUSTERS

n	Bonding	Non-bonding
4 (T_d)	$S^\sigma(a_1)P^\sigma(t_2)$	$D_0^\pi/\overline{D}_0^\pi(e)$
6 (D_{3h})	$S^\sigma(a_1')P^\sigma(a_2''+e')D_0^\pi(a_1')$	$D_{1s,1c}^\pi(e'')\overline{D}_{1s,1c}^\pi(e')$
8 (O_h)	$S^\sigma(a_{1g})$, $P^\sigma(t_{1u})$, $D_{0,2s}^\pi(e_g)$	$D_{1s,1c,2c}^\pi(t_{2g})$
		$\overline{D}_{1s,1c,2c}^\pi(t_{2u})$
10 (D_{5h})	$S^\sigma(a_1')P^\sigma(a_2''+e_1')$	$D_{1s,1c}^\pi(e_1'')F_{2s,2c}^\pi(e_2'')$
	$D_0^\pi(a_1')$, $D_{2s,2c}^\pi(e_2')$	$\overline{D}_{1s,1c}^\pi(e_1')\overline{F}_{2s,2c}^\pi(e_2')$
12 (D_{6h})	$S^\sigma(a_{1g})P^\sigma(a_{2u}+e_{1u})$	$D_{1s,1c}^\pi(e_{1g})F_{2s,2c}^\pi(e_{2u})$
	$D_0^\pi(a_{1g})$, $D_{2s,2c}^\pi(e_{2g})F_{3s}^\pi(b_{1g})$	$F_{3c}^\pi(b_{2g})$
		$\overline{D}_{1s,1c}^\pi(e_{1u})\overline{F}_{2s,2c}^\pi(e_{2g})$
		$\overline{F}_{3c}^\pi(b_{2u})$

References

1 K. Wade, Adv. Inorg. and Radiochem., 18 (1976) 1.
2 D.M.P. Mingos, Nature, Phys. Sci., 236 (1972) 99.
3 D.M.P. Mingos, J. Chem. Soc., Chem. Commun., (1983) 706; and Acc. Chem. Res., 17 (1984) 311.
4 R.B. King and D.H. Rouvray, J. Amer. Chem. Soc., 99 (1977) 7834.
5 M.J. McGlinchey and Y. Tal, Chemical Applications of Topology and Graph Theory, in Studies in Phys. and Theor. Chem., 28 (1983) 124 and references therein.
6 A.J. Stone, Mol. Phys., 41 (1980) 1339.
7 A.J. Stone, Inorg. Chem., 20 (1981) 563.
8 A.J. Stone and M.J. Alderton, Inorg. Chem., 21 (1982) 2297.
9 A.J. Stone, Polyhedron, in press.
10 M. Elian, M.M.L. Chen, D.M.P. Mingos and R. Hoffmann, Inorg. Chem., 15 (1976) 1148; and R. Hoffmann, Angew. Chem., Int. Ed. Engl., 21 (1982) 711.
11 P. Brint, J.P. Cronin and E. Seward, J. Chem. Soc., Dalton Trans., (1983) 675.
12 (a) $C_4Bu^t_4$; G. Maier, S. Pfriem, U. Schafter and R. Matusch, Angew. Chem., 90 (1978) 652; (b) C_6H_6; T.J. Katz and N. Acton, J. Amer. Chem. Soc., 95 (1973) 2738; (c) C_8H_8; P.E. Eaton and T.V. Cole, J. Amer. Chem. Soc., 86 (1973) 3157; (d) $C_{10}H_{10}$; P.E. Eaton, Y.S. Or and S.J. Branca, J. Amer. Chem. Soc., 103 (1981) 2134; (e) $C_{20}H_{20}$; R.J. Ternansky, D.W. Balogh and L.A. Paquette, J. Amer. Chem. Soc., 104 (1982) 4503.
13 S.F.A. Kettle, Theor. Chim. Acta, 14 (1969) 175 and references therein.
14 MO Calculations on C_nH_n Polyhedra: (a) C_8H_8; J.M. Schulman, C.R. Fischer, P. Soloman and T.J. Venanzi, J. Amer. Chem. Soc., 100 (1978) 2949; (b) C_4H_4; J.M. Schulman and T.J. Venanzi, J. Amer. Chem. Soc., 96 (1974) 4739; also E. Heilbronner, T.B. Jones, A. Kreks, K.-D. Malsch, G. Maier, J. Pocklington and A. Schmelzer, J. Amer. Chem. Soc., 102 (1980) 564; (c) C_6H_6; M.D. Newton, J.M. Schulman and M.M. Manus. J. Amer. Chem. Soc., 96 (1974) 17; (d) $C_{20}H_{20}$; J.M. Schulman, T.J. Venanzi and R.L. Disch, J. Amer. Chem. Soc., 97 (1975) 5335.
15 (a) M.R. Churchill and J.P. Hutchinson, Inorg. Chem., 17 (1978) 3528; (b) V.G. Albano, D. Braga and S. Martinengo, J. Chem. Soc., Dalton Trans., (1981) 717; (c) L.D. Lower and L.F. Dahl, J. Amer. Chem. Soc., 98 (1976) 5046; (d) C.T.W. Chu, PhD. Thesis, Univ. Wisconsin (Madison) (1977).
16 M.I. Forsyth and D.M.P. Mingos, J. Chem. Soc., Dalton Trans., (1977) 610.
17 (a) P.F. Jackson, B.F.G. Johnson, J. Lewis, B.E. Reichert and G.M. Sheldrick, J. Chem. Soc., Chem. Commun., (1976) 271; (b) R. Mason, K.M. Thomas and D.M.P. Mingos, J. Amer. Chem. Soc., 95 (1973) 3802; (c) M.I. Bruce and B.K. Nicholson, J. Chem. Soc. Chem. Commun., (1982) 1141; (d) V.G. Albano, D. Braga, S. Martinengo, P. Chini, M. Sansoni and D. Strumulo, J. Chem. Soc., Dalton Trans., (1980) 52; (e) S. Martinengo, G. Ciani, A. Sironi and P. Chini, J. Amer. Chem. Soc., 100 (1978) 7096.
18 K. Wade and M.E. O'Neill, Polyhedron, 2 (1983) 963.
19 S.C. Critchlow and J.D. Corbett, J. Amer. Chem. Soc., 105 (1983) 5715.
20 V.G. Albano, M. Sansoni, P. Chini, S. Martinengo and D. Strumulo, J. Chem. Soc., Dalton Trans., (1976) 970.